Inorg. Chem. **2002**, *41*, 2441–2450

Tetranuclear Manganese Complexes with Dimer-of-Dimer and Ladder Structures from the Use of a Bis-Bipyridyl Ligand

E. Carolina Sañudo,[†] Vincent A. Grillo,[†] Michael J. Knapp,[‡] John C. Bollinger,[†] John C. Huffman,[†] David N. Hendrickson,*[,‡] and George Christou*[,†,§]

Department of Chemistry and Molecular Structure Center, Indiana University, Bloomington, Indiana 47405-7102, and Department of Chemistry, University of California at San Diego, La Jolla, California 92093-0358

Received December 10, 2001

The reaction of the bis-chelating ligand 1,2-bis(2,2′-bipyridine-6-yl)ethane (L) with the trinuclear species of formula $[Mn_3O(O_2CR)_6(py)_3](ClO_4)$ (R = Me (**1**); R = Et (**2**); R = Ph (**3**)) has afforded the new tetranuclear mixed-valent complexes $[Mn_4O_2(O_2CR)_4L_2](ClO_4)_2$ (R = Me (**4**); R = Et (**5**); R = Ph (**6**)) and $[Mn_4O_2(OMe)_3(O_2CR)_2L_2(MeOH)](ClO_4)_2$ (R = Me (**7**); R = Et (**8**); R = Ph (**9**)). Complexes **4**–**6** were obtained in yields of 20%, 44%, and 37%, respectively. They are mixed-valent, with an average Mn oxidation state of +2.5. Complexes **7**–**9** were obtained in yields of 57%, 65%, and 70%, respectively. They are also mixed-valent, but with an average Mn oxidation state of +2.75. Complexes **4**·2THF and **9**·3MeOH·H_2O crystallize in the triclinic space group $P\bar{1}$ and contain $[Mn_4(\mu_3\text{-}O)_2]^{6+}$ and $[Mn_4(\mu_3\text{-}O)_2(\mu\text{-}OMe)_2]^{5+}$ cores, respectively, the latter being a new structural type in the family of Mn_4 complexes. Reactivity studies of **4**–**9** have shown that **4**–**6** can be converted into **7**–**9**, respectively, and vice versa. The magnetic properties of **5** and **9** have been studied by dc and ac magnetic susceptibility techniques. Complex **5** displays antiferromagnetic coupling between its Mn ions resulting in a spin ground state of $S = 0$. Complex **9** also displays antiferromagnetic coupling, but the resulting ground state is $S = {}^7/_2$, as confirmed by fitting magnetization versus field data collected for **9** at low temperatures, which gave $S = {}^7/_2$, $D = -0.77$ cm^{-1}, and $g = 1.79$. Complex **9** exhibits a frequency-dependent out-of-phase ac susceptibility peak, indicative of the slow magnetization relaxation that is diagnostic of single-molecule magnetism behavior.

Introduction

For a number of years, we have been engaged in developing metal cluster chemistry with oxide bridges and predominantly carboxylate peripheral ligation.[1] These efforts have often also involved the use of chelating ligands such as 2,2′-bipyridine (bpy), 2-picolinate (pic^-), and the anion of dibenzoylmethane (dbm^-), and a variety of polynuclear metal clusters have been obtained with metal nuclearities ranging from 2 to 11.[2] We have mainly focused on manganese for two reasons: First, Mn is biologically relevant, being present at the active site of many metallobiomolecules,[3] perhaps the most important being the water oxidizing complex (WOC) of Photosystem II, the species in plants (and cyanobacteria) that oxidizes water to dioxygen.[4]

* Authors to whom correspondence should be addressed. E-mail: christou@chem.ufl.edu (G.C.); dhendrickson@ucsd.edu (D.N.H.).
† Indiana University.
‡ University of California at San Diego.
§ Present address: Department of Chemistry, University of Florida, Gainesville, FL 32611-7200.

(1) Aromi, G.; Aubin, S. M. J.; Bolcar, M. A.; Christou, G.; Eppley, H. J.; Folting, K.; Hendrickson, D. N.; Huffman, J. C.; Squire, R. C.; Tsai, H. L.; Wang, S.; Wemple, M. W. *Polyhedron* **1998**, *17*, 3005.
(2) (a) Li, Q.; Vincent, J. B.; Chang, H. R.; Huffman, J. C.; Boyd, P. D. W.; Christou, G.; Libby, E.; Hendrickson, D. N. *Angew. Chem., Intl. Ed. Engl* **1988**, *27*, 1731. (b) Libby, E.; Webb, R. J.; Streib, W. E.; Folting, K.; Huffman, J. C.; Christou, G. *J. Chem. Soc., Chem. Commun*. **1989**, 1411. (c) Vincent, J. B.; Christmas, C.; Chang, H. R.; Li, Q.; Boyd, P. D. W.; Huffman, J. C.; Hendrickson, D. N.; Christou, G. *J. Am. Chem. Soc*. **1989**, *111*, 2086. (d) Christou, G.; Perlepes, S. P.; Folting, K.; Huffman, J. C.; Webb, R. J.; Hendrickson, D. N. *J. Chem. Soc. Chem. Commun*. **1990**, 746. (e) Wang, S.; Folting, K.; Streib, W. E.; Schmitt, E. A.; McCusker, J. K.; Hendrickson, D. N.; Christou, G. *Angew. Chem., Int. Ed. Engl*. **1991**, *30*, 305. (f) Libby, E.; McCusker, J. K.; Schmitt, E. A.; Folting, K.; Hendrickson, D. N.; Christou, G. *Inorg. Chem.* **1991**, *30*, 3486. (g) Perlepes, S. P.; Huffman, J. C.; Christou, G. *J. Chem. Soc., Chem. Commun.* **1991**, *23*, 1657. (h) Wang, S.; Tsai, H. L.; Streib, W. E.; Christou, G.; Hendrickson, D. N. *J. Chem. Soc., Chem. Commun.* **1992**, 677. (i) Eppley, H. J.; Aubin, S. J.; Streib, W. E.; Bollinger, J. C.; Hendrickson, D. N.; Christou, G. *Inorg. Chem.* **1997**, *36*, 109.
(3) *Manganese Redox Enzymes*; Pecoraro, V. L., Ed.; VCH Publishers: New York, 1992.
(4) Yachandra, V. K.; Sauer, K.; Klein, M. P. *Chem. Rev.* **1996**, *96*, 2927.

10.1021/ic011262k CCC: $22.00
Published on Web 03/30/2002

The WOC is known to be a tetranuclear Mn cluster of yet unknown structure.[5] Second, Mn clusters often display large, and sometimes abnormally large, spin (*S*) values in the ground state, and this combined with a large anisotropy has led some of these species to be single-molecule magnets (SMMs).[6] These are individual molecules that display the ability to function as magnetizable magnets below their blocking temperature.[7]

Poly-pyridyl groups have had a major impact over many years on the field of supramolecular chemistry, where they have been employed as "programmed" components in self-assembly reactions with mononuclear metal centers. This has led to a variety of metal/ligand supramolecular ensembles being obtained such as double and triple helices, grids, ladders, and so forth.[8] In our own work, we have previously employed such groups in amalgamation with our metal cluster chemistry to access new structural types of clusters as well as assemblies of multiple components as a supramolecular assembly. For example, the use of the bis-chelating ligand 1,2-bis(2,2′-bipyridine-6-yl)ethane (L) in such a hybrid approach, involving reactions with cobalt or iron carboxylate clusters, has yielded the new 4Co(II), 4Co(III) complex $[Co_8O_4(OH)_4(O_2CMe)_6L_2]^{2+}$,[9] possessing a face-sharing triple-cubane structure, and the Fe(III) clusters $[Fe_6O_4Cl_4(O_2CPh)_4L_2]^{2+}$ and $[Fe_6O_6(O_2CPh)_3(H_2O)_2L_2]^{3+}$,[10] containing ladderlike cores, among others.[11,12] The cores of these

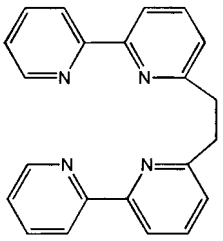

L

complexes can be described as the result of linking several dinuclear $[M_2O_2]$ units, either face-to-face (triple-cubane structure) or edge-to-edge (ladder structure). These prior results encouraged us to extend this use of L to Mn carboxylate chemistry, and we have thus been exploring the reactions of L with suitable Mn starting materials. The results of this investigation are reported here.[12]

Experimental Section

Syntheses. All manipulations were performed under aerobic conditions except the synthesis of bis(bipyridine) ligand L, which was carried out as described elsewhere.[13] All chemicals were used as received. $[Mn_3O(O_2CR)_6(py)_3](ClO_4)$ (R = Me (**1**), Et (**2**), and Ph (**3**)) were available from previous work.[14]

$[Mn_4O_2(O_2CMe)_4L_2](ClO_4)_2$ (4). Method A. Solid L (0.30 g, 0.90 mmol) was added to a stirred solution of complex **1** (0.52 g, 0.60 mmol) in MeCN (60 mL), which caused a rapid color change from dark brown to dark brown-red as the solid dissolved. The solution was maintained at room temperature overnight and filtered, and the filtrate layered with an equal volume of THF. After several days, dark red microcrystals of **4**·2THF were collected by filtration, washed with THF, and dried in air; yield 20%. Some layerings produced crystals suitable for X-ray crystallography. Anal. Calcd (found) for **4**·2THF ($C_{60}H_{64}Cl_2Mn_4N_8O_{20}$): C, 47.79 (47.38); H, 4.28 (4.26); N, 7.43 (7.43). Selected IR data (KBr pellet, cm^{-1}): 1598 (s), 1582 (vs), 1566 (s), 1453 (s), 1425 (s), 1091 (vs), 1029 (m), 1019 (m), 1005 (m), 781 (s), 669 (m), 654 (s), 623 (s), 604 (m).

Method B. Solid L (0.10 g, 0.30 mmol) was added to a stirred solution of $Mn(O_2CMe)_2 \cdot 4H_2O$ (0.072 g, 0.30 mmol) and complex **1** (0.084 g, 0.10 mmol) in MeCN (20 mL). After 1 h, the red solution was filtered, the filtrate mixed with an equal volume of THF containing $NBu^n_4ClO_4$ (0.066 g, 0.20 mmol), and the solution maintained at room temperature overnight. The dark red precipitate was collected by filtration, washed with THF, and dried in vacuo; yield 30%. The material was spectroscopically identical with material from Method A.

Method C. $NBu^n_4MnO_4$ (0.070 g, 0.19 mmol) in MeCN (3 mL) was added to a slurry of $Mn(O_2CMe)_2 \cdot 4H_2O$ (0.28 g, 1.2 mmol) and L (0.23 g, 0.68 mmol) in $MeCN/MeCO_2H$ (20 mL/4 mL) to produce a dark red solution. After 10 min, $NBu^n_4ClO_4$ (0.30 g, 0.87 mmol) was added, followed by an equal volume of THF. After one week, dark red crystals were collected by filtration, washed with THF, and dried in vacuo; yield 20%. The material was spectroscopically identical with that from Method A.

$[Mn_4O_2(O_2CEt)_4L_2](ClO_4)_2$ (5). This was prepared by Method A for complex **4** using $[Mn_3O(O_2CEt)_6(py)_3](ClO_4)$ (**2**). Slow crystallization yielded brown crystals of **5**·2THF. The yield was ~44%. Anal. Calcd (found) for **5**·2THF ($C_{64}H_{72}Cl_2Mn_4N_8O_{20}$): C, 49.15 (49.11); H, 4.64 (4.59); N, 7.16 (7.16). Faster precipitation afforded microcrystalline samples that analyzed for **5**·2MeCN. Anal. Calcd (found) for **5**·2MeCN ($C_{58}H_{70}Cl_2Mn_4N_{10}O_{18}$): C, 47.98 (48.20); H 4.78 (4.59); N 9.33 (8.99).

(5) Jordan, P.; Fromme, P.; Witt, H. T.; Klukas, O.; Saenger, W.; Krauss, N. *Nature* **2001**, *411*, 909.

(6) Christou, G.; Gatteschi, D.; Hendrickson, D. N.; Sessoli, R. *MRS Bull.* **2000**, *25*, 66.

(7) (a) Sessoli, R.; Tsai, H. L.; Schake, A. R.; Wang, S.; Vincent, J. B.; Folting, K.; Gatteschi, D.; Hendrickson, D. N.; Christou, G. *J. Am. Chem. Soc.* **1993**, *115*, 1804. (b) Sessoli, R.; Gatteschi, D.; Novak, M. A.; Caneschi, A. *Nature* **1993**, 141. (c) Eppley, H. J.; Tsai, H. L.; de Vries, N.; Folting, K.; Hendrickson, D. N.; Christou, G. *J. Am. Chem. Soc.* **1995**, *120*, 301. (d) Aliaga, N.; Folting, K.; Hendrickson, D. N.; Christou, G. *Polyhedron* **2001**, *20*, 1273. (e) Soler, M.; Chandra, S. W.; Ruiz, D.; Huffman, J. C.; Hendrickson, D. N.; Christou, G. *Polyhedron* **2001**, *20*, 1279. (f) Maccaagnano, S.; Achey, R.; Negusse, E.; Lussier, A.; Mola, M. M.; Hill, S.; Dalal, N. S. *Polyhedron* **2001**, *20*, 1441.

(8) (a) Lehn, J. N. *Supramolecular Chemistry;* VCH Publishers: New York, 1995. (b) Ferrere, S.; Elliott, C. M. *Inorg. Chem.* **1995**, *34*, 5818. (c) Youinou, M. T.; Ziessel, R.; Lehn, J. M. *Inorg. Chem.* **1991**, *30*, 2144. (d) Piguet, C.; Berbardinelli, G.; Hopfgartner, G. *Chem. Rev.* **1997**, *97*, 2005. (e) Constable, E. C. *Chem. Commun.* **1997**, 1703. (f) Baxter, P.; Lehn, J. M.; De Cian, A.; Fischer, J. *Angew. Chem., Intl. Ed. Engl.* **1993**, *32*, 69. (g) Hasenknopf, B.; Lehn, J. M.; Boumediene, N.; Dupont-Gervais, A.; Van Dorsselaer, A.; Kneisel, B.; Fenske, D. *J. Am. Chem. Soc.* **1997**, *119*, 10956. (h) Berl, V.; Huc, I.; Khoury, R. G.; Lehn, J. M. *Eur. J. Chem.* **2001**, *7*, 2798. (i) Albrecht, M. *Chem. Rev.* **2001**, *101*, 3457.

(9) Grillo, V. A.; Sun, K.; Folting, K.; Hendrickson, D. N.; Christou, G. *J. Chem. Soc., Chem. Commun.* **1996**, 2233.

(10) (a) Grant, C. M.; Knapp, M. J.; Huffman, J. C.; Hendrickson, D. N.; Christou, G. *Inorg. Chem.* **1968**, *7*, 6065. (b) Seddon, E. J.; Yoo, J.; Folting, K.; Huffman, J. C.; Hendrickson, D. N.; Christou, G. *J. Chem. Soc., Dalton Trans.* **2000**, 3640.

(11) Grant, C. M.; Stamper, B. J.; Knapp, M. J.; Folting, K.; Hendrickson, D. N.; Christou, G. *J. Chem. Soc., Dalton Trans.* **1999**, 3399.

(12) Grillo, V. A.; Knapp, M.; Bollinger, J. C.; Hendrickson, D. N.; Christou, G. *Angew. Chem., Intl. Ed. Engl.* **1996**, *35*, 1818.

(13) Garber, T.; Van Wallendael, S.; Rillema, D. P.; Kirk, M.; Hatfield, W. E.; Wech, J. H. *Inorg. Chem.* **1990**, *29*, 2863.

(14) Vincent, J. B.; Chang, H. R.; Folting, K.; Huffman, J. C.; Hendrickson, D. N.; Christou, G. *J. Am. Chem. Soc.* **1987**, *109*, 5703.

$[Mn_4O_2(O_2CPh)_4L_2](ClO_4)_2$ (6). This was prepared by Method A for complex **4** using $[Mn_3O(O_2CPh)_6(py)_3](ClO_4)$ (**3**). The yield was ∼37%. Anal. Calcd (found) for **6**·THF·H_2O ($C_{76}H_{66}Cl_2Mn_4N_8O_{20}$): C, 53.63 (53.88); H, 3.91 (3.95); N, 6.58 (6.84).

Conversion of 4 to 6. The ligand substitution was effected by treatment of **4** in MeCN with 4 equiv of $PhCO_2H$, followed by two cycles of addition of toluene and solvent removal in vacuo. This produced a red powder identified spectroscopically as **6** in essentially quantitative yield.

$[Mn_4O_2(OMe)_3(O_2CMe)_2L_2(MeOH)](ClO_4)_2$ (7). Method A. Solid L (0.10 g, 0.30 mmol) was added to a stirred solution of complex **1** (0.17 g, 0.20 mmol) in MeOH (50 mL). The slurry was stirred at ∼60 °C for 2 h, and the resulting red solution was left undisturbed for 2 days to give dark red crystals. These were collected by filtration, washed with a little MeOH, and dried in air; yield, 57%. Anal. Calcd (found) for **7**·H_2O ($C_{52}H_{58}Cl_2Mn_4N_8O_{19}$): C, 44.94 (44.95); H, 4.21 (4.17); N, 8.06 (7.62).

$[Mn_4O_2(OMe)_3(O_2CEt)_2L_2(MeOH)](ClO_4)_2$ (8). This was prepared in an analogous manner to **7** by using complex **2**. The yield was 55%. Anal. Calcd (found) for **8** ($C_{54}H_{60}Cl_2Mn_4N_8O_{18}$): C, 46.34 (46.26); H, 4.32 (4.18); N, 8.01 (7.71).

$[Mn_4O_2(OMe)_3(O_2CPh)_2L_2(MeOH)](ClO_4)_2$ (9). This was prepared in an analogous manner to **7** using complex **3** and was obtained as dark red crystals suitable for crystallography. The yield was 70%. Anal. Calcd (found) for **9**·2H_2O ($C_{62}H_{64}Cl_2Mn_4N_8O_{20}$): C, 48.61 (48.54); H, 4.21 (4.32); N, 7.31 (7.60). Selected IR data (cm^{-1}): 1599 (s), 1573 (m), 1550 (s), 1454 (s), 1398 (s), 779 (s), 723 (m), 688 (m), 673 (s), 652 (m), 641 (m), 622 (s), 585 (m).

X-ray Crystallography. Data for **4**·2THF were collected by the moving crystal, moving detector technique with fixed background counts at each extreme of the scan. Data were corrected for Lorentz and polarization effects, and equivalent data were averaged. The structure was solved by direct methods (MULTAN78) and Fourier techniques. Hydrogen atoms were located in a difference map phased on the non-hydrogen atoms and included as isotropic contributors in the final least-squares cycles. A final difference Fourier map was featureless, with the largest peak having an intensity of 0.43 e/Å^3 and residing near a solvent molecule.

The Bruker-AXS SMART 6000 system was used for data collection on **9**·3MeOH·H_2O. The data were collected using 10 s frames with an ω scan of 0.30°. Data were corrected for Lorentz and polarization effects and equivalent reflections averaged using the Bruker SAINT software as well as utility programs from the XTEL library. The structure was readily solved using SHELXTL and Fourier techniques. The asymmetric unit consists of one unique molecule and a second lying at a center of inversion (triclinic, $Z = 3$). There are two perchlorate anions per cation (three independent anions per asymmetric unit), in addition to both methanol and water molecules of crystallization. Many of the hydrogen atoms were visible in a difference Fourier map phased on the non-hydrogen atoms. All hydrogen atoms were placed in idealized calculated positions and treated as fixed atom contributors in the final cycles of refinement. A final difference Fourier map was essentially featureless, although there were several peaks in the vicinity of the solvent molecules in the lattice. The largest peak was 1.56 e/Å^3.

Physical Measurements. IR spectra were recorded on KBr pellets using a Nicolet 510P spectrophotometer. ^{1}H NMR spectra were recorded on a Varian XL-300 spectrometer with the solvent protio impurity signal as an internal reference. Direct current and alternating current magnetic susceptibility data were collected on microcrystalline samples (restrained in eicosane to prevent torquing) using a Quantum Design MPMS-XL SQUID magnetometer equipped with a 7 T magnet. A diamagnetic correction to the observed susceptibilities was applied using Pascal's constants.

Results and Discussion

Syntheses and Reactivity. The syntheses and transformations of complexes **4** and **9** described in this work are summarized for convenience in Scheme 1. The reaction of $[Mn_3O(O_2CMe)_6(py)_3](ClO_4)$ (**1**) with 1.5 equiv of the bis-bipyridyl ligand L in MeCN leads to the formation of $[Mn_4O_2(O_2CMe)_4L_2](ClO_4)_2$ (**4**). Addition of THF to the reaction mixture results in the formation of red-orange crystals, which can be isolated after a few days. Its structure was determined by X-ray crystallography. Analogues of starting complex **1** containing other carboxylate groups (**2**, R = Et and **3**, R = Ph) are also available, and these have allowed the preparation of $[Mn_4O_2(O_2CEt)_4L_2](ClO_4)_2$ (**5**) and $[Mn_4O_2(O_2CPh)_4L_2](ClO_4)_2$ (**6**) following similar procedures to that used for **4**. Both products can be isolated as crystalline solids upon addition of an equal volume of THF to the MeCN reaction solution. They have been characterized by ^{1}H NMR and IR spectroscopies and elemental analysis; structural characterization was not attempted owing to the expected similarity to **4**. It was also possible to obtain complex **4** by reaction of $Mn(O_2CMe)_2$ tetrahydrate with $TBAMnO_4$ in MeCN in the presence of ligand L (method C); this is in fact an in situ preparation of the trinuclear cluster **1**.[14] The yield was comparable to that obtained from reaction of the trinuclear Mn cluster **1** with the ligand (method A).

It is possible to obtain complex **6** directly from **4** by using a carboxylate substitution procedure, as applied on previous occasions to various manganese−carboxylate clusters.[7c,15] Thus, an MeCN solution of **4** was treated with 4 equiv of benzoic acid, and this gave a quantitative yield of **6** after removal of the acetic acid as its azeotrope with toluene (eq 1).

$$[Mn_4O_2(O_2CMe)_4L_2]^{2+} + 4PhCO_2H \rightarrow [Mn_4O_2(O_2CPh)_4L_2]^{2+} + 4MeCO_2H \quad (1)$$

In previous studies of the reactions of iron(III) carboxylate complexes with L, it was found that the identity of the product was very dependent on the solvent employed.[10] Thus, the reactions that lead to **4**−**6** in MeCN were also carried out in MeOH, and the products were now the species $[Mn_4O_2(OMe)_3(O_2CR)_2L_2(MeOH)](ClO_4)_2$ (R = Me (**7**), Et (**8**), Ph (**9**)). The presence of bridging MeO^- groups was confirmed crystallographically for **9** (vide infra), and this parallels the similar incorporation of bridging MeO^- groups in iron(III)/L chemistry when reactions are carried out in MeOH. Note that **4**−**6** are 2Mn(II), 2Mn(III), whereas **7**−**9** are Mn(II), 3Mn(III).

The reaction of L with trinuclear Mn carboxylate clusters thus yields tetranuclear Mn products in both MeCN and MeOH, but the average Mn oxidation state is different in the two cases. For both **4**−**6** and **7**−**9**, however, the product

(15) Sessoli, R.; Tsai, H. L.; Schake, A. R.; Wang, S.; Vincent, J. B.; Folting, K.; Gatteschi, D.; Hendrickson, D. N.; Christou, G. *J. Am. Chem. Soc.* **1993**, *115*, 1804.

Scheme 1

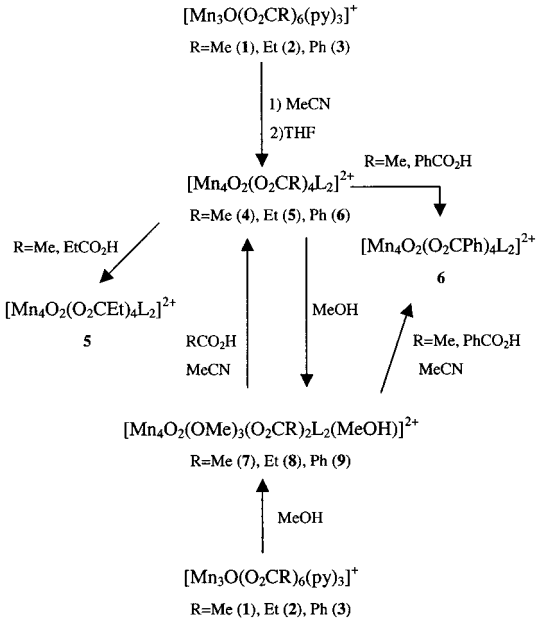

oxidation level is lower than that of starting complexes **1**−**3** (3Mn(III)). In some reactions with other chelating ligands such 2-hydroxymethylpyridine, oxidation of the chelate provides the reducing equivalents to lower the metal oxidation state of the product,[16] but because L is not easily oxidized, the origin of the Mn(II) in **4**−**9** was addressed further using the benzoate reaction systems. The filtrates after isolation of **6** and **9** were concentrated, and solid was isolated that was identified as $[Mn_{12}O_{12}(O_2CPh)_{16}(H_2O)_2]$ by spectroscopic comparison with authentic material.[15] This byproduct is also mixed-valent, 8Mn(III), 4Mn(IV), and it suggests that a disproportionation of Mn(III) is occurring during the reaction (eq 2). On this basis, it was suspected that addition of a Mn(II) reagent to the reaction

$$20[Mn_3^{III}] \rightarrow 6[Mn_2^{II}Mn_2^{III}] + 3[Mn_8^{III}Mn_4^{IV}] \qquad (2)$$

might improve the yield, and this was investigated for the acetate reaction system leading to **4**. Indeed, it was found that the addition of $Mn(O_2CMe)_2 \cdot 4H_2O$ to the reaction mixture led to a small but nevertheless significant improvement in the yield from 20% to 30%.

Although no assignment of the signals in the ^{1}H NMR spectra of complexes **4**−**6** and **7**−**9** has been attempted because of their very broad and poorly resolved nature, the NMR profiles can nevertheless be used as fingerprint spectra to distinguish the two types of complex. This allowed the following transformations to be identified (eq 3). Compounds **4**−**6** can be converted into **7**−**9** by dissolution in MeOH.

$$[Mn_4O_2(O_2CR)_4(L)_2]^{2+} + 4MeOH \underset{-e^-}{\overset{+e^-}{\rightleftharpoons}} [Mn_4O_2(OMe)_3(O_2CR)_2(L)_2(MeOH)]^{2+} + 2RCO_2H + H^+ \qquad (3)$$

For example, if **5** is dissolved in CD_3OD in an NMR tube, the ^{1}H NMR spectrum is identical with that of **8** measured separately. The conversion is reversible, and removal of the methanol in vacuo drives the equilibrium back to the left-hand side and regenerates starting material: removal of the CD_3OD and dissolution of the resulting solid in CD_3CN gives a ^{1}H NMR spectrum identical with that of **5**. Its infrared spectrum is also identical with that of **5**. Similarly, addition of carboxylic acid to compounds **7**−**9** in MeCN transforms them quantitatively into **4**−**6,** respectively, as indicated by ^{1}H NMR monitoring of the reactions and confirmed by spectroscopic (IR, ^{1}H NMR) investigation of isolated solids. Presumably, the necessary redox changes are facilitated by O_2 reduction or MeOH oxidation.

Table 1. Crystallographic Data for Complexes **4**·2THF and **9**·3MeOH·H_2O

	4	**9**
formula[a]	$C_{60}H_{64}Cl_2Mn_4N_8O_{20}$	$C_{62}H_{59}Cl_2Mn_4N_8O_{18}$
fw, g/mol	1507.87	1607.98
space group	$P\bar{1}$	$P\bar{1}$
a, Å	12.017(2)	14.219(1)
b, Å	12.197(2)	19.116(1)
c, Å	12.343(2)	20.905(1)
α, deg	73.29(1)	74.71(1)
β, deg	78.02(1)	83.75(1)
γ, deg	68.36(1)	68.74(1)
V, Å^3	1600	5107
Z	1	3
T, °C	−169	−160
radiation, Å[b]	0.71069	0.71073
ρ_{calcd}, g/cm^3	1.565	1.568
μ, cm^{-1}	9.020	8.866
R^c (R_w)[d], %	4.48 (4.19)	6.12 (5.11)

[a] Including solvate molecules. [b] Graphite monochromator. [c] $R = 100\sum||F_o|-|F_c||/\sum|F_o|$. [d] $R_w = 100[\sum w(|F_o| - |F_c|)^2/\sum w|F_o|^2]^{1/2}$ where $w = 1/\sigma^2(|F_o|)$.

Description of Structures

Crystallographic data collection and structure refinement details for **4**·2THF and **9**·3MeOH·H_2O are summarized in Table 1.

$[Mn_4O_2(O_2CMe)_4L_2](ClO_4)_2$ (4). A labeled ORTEP plot of the cation of **4** is shown in Figure 1, and selected interatomic distances and angles are listed in Table 2. Complex **4** crystallizes in triclinic space group $P\bar{1}$ with the molecule lying on an inversion center. There are two ClO_4^- anions per cation, and charge considerations indicate the cation to be mixed-valent, 2Mn(II), 2Mn(III). The cation consists of two $[Mn_2O(O_2CMe)_2L]^+$ fragments held together by interfragment linkages Mn(1)−O(3′) and Mn(1′)−O(3) (1.879(1) Å), and the intramolecular π-stacking of the bipyridine rings of the ligand L at a distance of 3.5 Å. Two of the metal centers are hexacoordinated (Mn(1) and Mn(1′)), and the other two are pentacoordinated (Mn(2) and Mn(2′)). The geometry at Mn(2) and Mn(2′) is very distorted trigonal bipyramid (tbp), with a τ value of 0.61 ($\tau = 0$ for square pyramid (sp) and 1 for tbp).[17a] The bond distances around

(16) (a) Boskovic, C.; Brechin, E. K.; Streib, W. E.; Folting, K.; Hendrickson, D. N.; Christou, G. *J. Chem. Soc., Chem. Commun.* **2001**, 467. (b) Boskovic, C.; Brechin, E. K.; Streib, W. E.; Folting, K.; Bollinger, J. C.; Hendrickson, D. N.; Christou, G. *J. Am. Chem. Soc.*, submitted for publication.

(17) (a) Schoonhoven, J. W. F. M.; Driessen, W. L.; Reedijk, J.; Verschoor, G. C. *J. Chem. Soc., Dalton Trans.* **1984**, 1053. (b) Blackman, A. G.; Huffman, J. C.; Lobkovsky, E. B.; Christou, G. *Polyhedron* **1992**, *11*, 251.

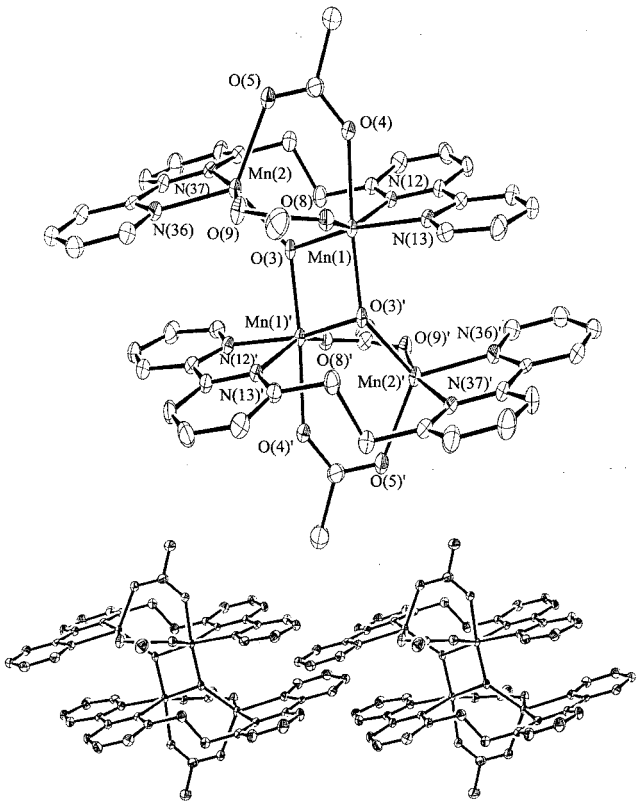

Figure 1. ORTEP representation and stereoview of the $[Mn_4O_2(O_2CMe)_4L_2]^{2+}$ cation of **4** at the 50% probability level.

Table 2. Selected Interatomic Distances (Å) and Angles (deg) for $[Mn_4O_2(O_2CMe)_4L_2](ClO_4)_2$ (**4**)

Mn(1)	Mn(1′)	2.784(4)	Mn(1)	N(12)	2.328(1)
Mn(1)	Mn(2)	3.208(4)	Mn(1)	N(13)	2.065(1)
Mn(1)	Mn(2′)	3.632(4)	Mn(2)	O(3)	2.030(1)
Mn(1)	O(3)	1.839(1)	Mn(2)	O(5)	2.082(1)
Mn(1′)	O(3)	1.879(1)	Mn(2)	O(9)	2.113(1)
Mn(1)	O(4)	2.032(1)	Mn(2)	N(36)	2.180(1)
Mn(1)	O(8)	2.179(1)	Mn(2)	N(37)	2.295(1)

O(3)	Mn(1)	O(3)	83.01(3)	N(12)	Mn(1)	N(13)	75.875(23)
O(3)	Mn(1)	O(4)	174.39(3)	O(3)	Mn(2)	O(5)	107.535(27)
O(3)	Mn(1)	O(4)	102.55(3)	O(3)	Mn(2)	O(9)	95.75(3)
O(3)	Mn(1)	O(8)	94.750(27)	O(3)	Mn(2)	N(36)	124.38(3)
O(3)	Mn(1)	O(8)	97.86(3)	O(3)	Mn(2)	N(37)	94.66(3)
O(3)	Mn(1)	N(12)	100.59(3)	O(5)	Mn(2)	O(9)	91.57(3)
O(3)	Mn(1)	N(12)	100.81(3)	O(5)	Mn(2)	N(36)	127.50(3)
O(3)	Mn(1)	N(13)	88.26(3)	O(5)	Mn(2)	N(37)	96.169(27)
O(3)	Mn(1)	N(13)	169.82(3)	O(9)	Mn(2)	N(36)	90.657(27)
O(4)	Mn(1)	O(8)	82.531(25)	O(9)	Mn(2)	N(37)	164.53(3)
O(4)	Mn(1)	N(12)	77.602(25)	N(36)	Mn(2)	N(37)	74.004(23)
O(4)	Mn(1)	N(13)	86.135(27)	Mn(1)	O(3)	Mn(1′)	96.99(3)
O(8)	Mn(1)	N(12)	157.08(3)	Mn(1)	O(3)	Mn(2)	111.93(3)
O(8)	Mn(1)	N(13)	91.604(25)	Mn(1)	O(3)	Mn(2)	136.601(25)

Mn(2), all >2 Å, are consistent with it being a Mn(II) center.[17b] On the basis of the structural parameters, the Mn(III) centers are hexacoordinated Mn(1) and Mn(1′), each of them clearly possessing a Jahn−Teller (JT) distortion in the form of an axial elongation along the O(8)−Mn(1)−N(12) axis. The JT axes at the two Mn(III) ions are nearly parallel. As expected, the JT axes are located so as to avoid the $Mn-O^{2-}$ bonds, which are the shortest and strongest in the molecule (<1.9 Å). Each Mn(II)−Mn(III) pair is quadruply bridged by O(3), two *syn*, *syn*-$MeCO_2^-$ groups, and the ligand L, which is attached to both metals.

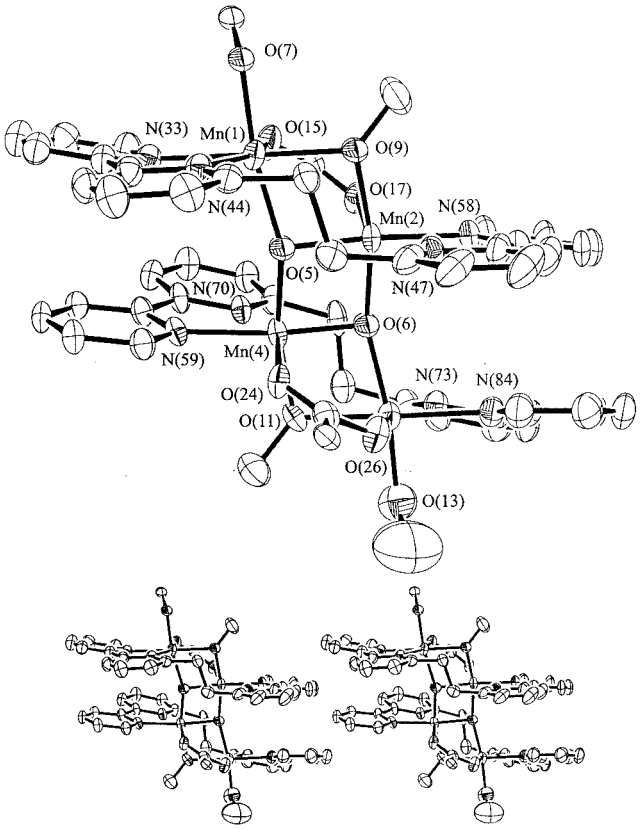

Figure 2. ORTEP representation and stereoview of the $[Mn_4O_2(OMe)_3(O_2CPh)_2L_2(MeOH)]^{2+}$ cation of **9** at the 50% probability level.

$[Mn_4O_2(OMe)_3(O_2CPh)_2L_2(MeOH)](ClO_4)_2$ (9). A labeled ORTEP plot of the cation of **9** is shown in Figure 2, and selected structural parameters are listed in Table 3. Complex **9** crystallizes in the triclinic space group $P\bar{1}$ with the cation in a general position. The structure of the cation consists of a ladderlike $[Mn_4O_4]$ core, with two of the oxygen atoms being from bridging MeO^- groups. The cation does not have any crystallographic symmetry, and all of the Mn centers possess a distorted octahedral geometry. Unlike the structure of **4**, the metric parameters of **9** were not consistent with a 2Mn(II), 2Mn(III) oxidation state description. A bond valence sum calculation[18] was therefore performed, and this suggested a Mn(II), 3Mn(III) situation. Indeed, Mn(2), Mn(3), and Mn(4) show clear evidence of the JT distortion expected for high-spin Mn(III) in near-octahedral geometry, taking the form of an axial elongation. One Mn(III)−N(L) bond distance at each metal is significantly longer (Mn(2)−N(47), Mn(3)−N(70), and Mn(4)−N(73); 2.338(4), 2.349(4), and 2.317(4) Å, respectively) than the other (Mn(2)−N(58), Mn(3)−N(59), and Mn(4)−N(84); 2.122(4), 2.100(4), and 2.169(4) Å, respectively). These bonds are trans to the longest Mn−O(O_2CPh) bonds in each case (Mn(2)−O(17), Mn(3)−O(24), and Mn(4)−O(26); 2.234(3), 2.229(3), and 2.125(3) Å, respectively, vs the typical 1.9 Å for a Mn(III)−O(carboxylate) bond). The three Jahn−Teller axes are aligned in a near parallel fashion. Again, the comparatively

(18) (a) Palenik, G. *Inorg. Chem.* **1997**, *36*, 4888. (b) Liu, W.; Thorp, H. H. *Inorg. Chem.* **1993**, *32*, 4102. (c) Brown, I. D.; Altermatt, D. *Acta Crystallogr., Sect. B* **1985**, 244.

Table 3. Selected Interatomic Distances (Å) and Angles (deg) for $[Mn_4O_2(OMe)_3(O_2CPh)_2L_2(MeOH)](ClO_4)_2$ (**9**)

Mn(1)	Mn(2)	2.991(1)	Mn(2)	N(47)	2.338(4)
Mn(2)	Mn(3)	2.810(1)	Mn(2)	N(58)	2.122(4)
Mn(3)	Mn(4)	2.941(1)	Mn(3)	O(5)	1.870(1)
Mn(1)	Mn(3)	3.772(1)	Mn(3)	O(6)	1.886(1)
Mn(2)	Mn(4)	3.794(1)	Mn(3)	O(11)	1.936(4)
Mn(1)	O(5)	1.989(1)	Mn(3)	O(24)	2.229(3)
Mn(1)	O(7)	1.987(1)	Mn(3)	N(59)	2.100(4)
Mn(1)	O(9)	2.100(1)	Mn(3)	N(70)	2.349(4)
Mn(1)	O(15)	2.113(4)	Mn(4)	O(6)	1.977(1)
Mn(1)	N(33)	2.227(4)	Mn(4)	O(11)	2.039(3)
Mn(1)	N(44)	2.282(4)	Mn(4)	O(13)	1.872(5)
Mn(2)	O(5)	1.894(1)	Mn(4)	O(26)	2.125(3)
Mn(2)	O(6)	1.891(1)	Mn(4)	N(73)	2.317(4)
Mn(2)	O(9)	1.924(1)	Mn(4)	N(84)	2.169(4)
Mn(2)	O(17)	2.234(3)			

O(5)	Mn(1)	O(7)	168.04(4)	O(5)	Mn(1)	N(44)	92.00(11)
O(5)	Mn(1)	O(9)	76.25 (3)	O(7)	Mn(1)	O(9)	93.51(4)
O(5)	Mn(1)	O(15)	93.69(11)	O(7)	Mn(1)	O(15)	92.31(11)
O(5)	Mn(1)	N(33)	103.97(1)	O(7)	Mn(1)	N(33)	86.67(11)
O(7)	Mn(1)	N(44)	85.75(11)	O(5)	Mn(3)	O(11)	166.27(10)
O(9)	Mn(1)	O(15)	89.26(9)	O(5)	Mn(3)	O(24)	95.13(10)
O(9)	Mn(1)	N(33)	176.03(12)	O(5)	Mn(3)	N(59)	90.57(12)
O(9)	Mn(1)	N(44)	110.42(10)	O(5)	Mn(3)	N(70)	97.29(11)
O(15)	Mn(1)	N(33)	86.77(14)	O(6)	Mn(3)	O(11)	82.34(9)
O(15)	Mn(1)	N(44)	160.30(14)	O(6)	Mn(3)	O(24)	95.78(8)
N(33)	Mn(1)	N(44)	73.55(15)	O(6)	Mn(3)	N(59)	173.80(13)
O(5)	Mn(2)	O(6)	83.19(3)	O(6)	Mn(3)	N(70)	103.95(9)
O(5)	Mn(2)	O(9)	82.84(3)	O(11)	Mn(3)	O(24)	85.49(14)
O(5)	Mn(2)	O(17)	92.49(8)	O(11)	Mn(3)	N(59)	103.16(15)
O(5)	Mn(2)	N(47)	110.54(11)	O(11)	Mn(3)	N(70)	86.80(14)
O(5)	Mn(2)	N(58)	173.32(13)	O(24)	Mn(3)	N(59)	87.59(14)
O(6)	Mn(2)	O(9)	165.91(4)	O(24)	Mn(3)	N(70)	157.64(13)
O(6)	Mn(2)	O(17)	97.30(10)	N(59)	Mn(3)	N(70)	73.80(14)
O(6)	Mn(2)	N(47)	98.03(11)	O(6)	Mn(4)	O(11)	77.57(10)
O(6)	Mn(2)	N(58)	90.91(12)	O(6)	Mn(4)	O(13)	168.97(16)
O(9)	Mn(2)	O(17)	85.09(10)	O(6)	Mn(4)	O(26)	92.79(10)
O(9)	Mn(2)	N(47)	85.24(11)	O(6)	Mn(4)	N(73)	94.54(11)
O(9)	Mn(2)	N(58)	103.14(13)	O(6)	Mn(4)	N(84)	100.39(12)
O(17)	Mn(2)	N(47)	153.62(14)	O(11)	Mn(4)	O(13)	92.75(18)
O(17)	Mn(2)	N(58)	85.12(15)	O(11)	Mn(4)	O(26)	92.26(13)
N(47)	Mn(2)	N(58)	73.30(16)	O(11)	Mn(4)	N(73)	106.57(14)
O(5)	Mn(3)	O(6)	83.95(3)	O(11)	Mn(4)	N(84)	177.87(16)
O(13)	Mn(4)	O(26)	92.85(17)	N(73)	Mn(4)	N(84)	74.08(16)
O(13)	Mn(4)	N(73)	83.07(17)	Mn(1)	O(5)	Mn(2)	100.74(3)
O(13)	Mn(4)	N(84)	89.34(19)	Mn(1)	O(5)	Mn(3)	155.55(3)
O(26)	Mn(4)	N(73)	160.87(13)	Mn(2)	O(5)	Mn(3)	96.60(3)
O(26)	Mn(4)	N(84)	87.23(15)	Mn(2)	O(6)	Mn(3)	96.14(3)
Mn(2)	O(6)	Mn(4)	157.37(3)	Mn(1)	O(9)	Mn(2)	95.92(3)
Mn(3)	O(6)	Mn(4)	99.11(3)	Mn(3)	O(11)	Mn(4)	95.40(15)

long bond distances observed for Mn(1), all 1.99 Å or greater, are in agreement with it being a Mn(II) ion.[17b] The Mn(1)−Mn(2) and Mn(3)−Mn(4) pairs are quadruply bridged by an oxide (O(5) and O(6)), a *syn, syn*-$PhCO_2^-$ group, the ligand L, and a MeO^- group. The phenyl rings of the carboxylate and bipyridine rings are essentially parallel (at a distance of ∼3.8 Å), providing intramolecular and intermolecular π-stacking interactions. All the Mn ions possess distorted octahedral geometry; Mn(1) and Mn(4) complete their coordination with a molecule of either MeO^- (Mn(4)) or MeOH (Mn(1)).

Compound **9** is a new structural type in the manganese−carboxylate family of clusters. Its Mn−oxide core is similar to the core of certain iron species with the ligand L,[10] containing the same four-rung (or greater) ladder motif.

Structural Comparison of $[Mn_4O_2]$ Complexes. The $[Mn_4(\mu_3\text{-}O)_2]^{6+}$ and $[Mn_4(\mu_3\text{-}O)_2(\mu\text{-}OMe)_2]^{5+}$ cores of the complexes obtained in this work are somewhat similar to

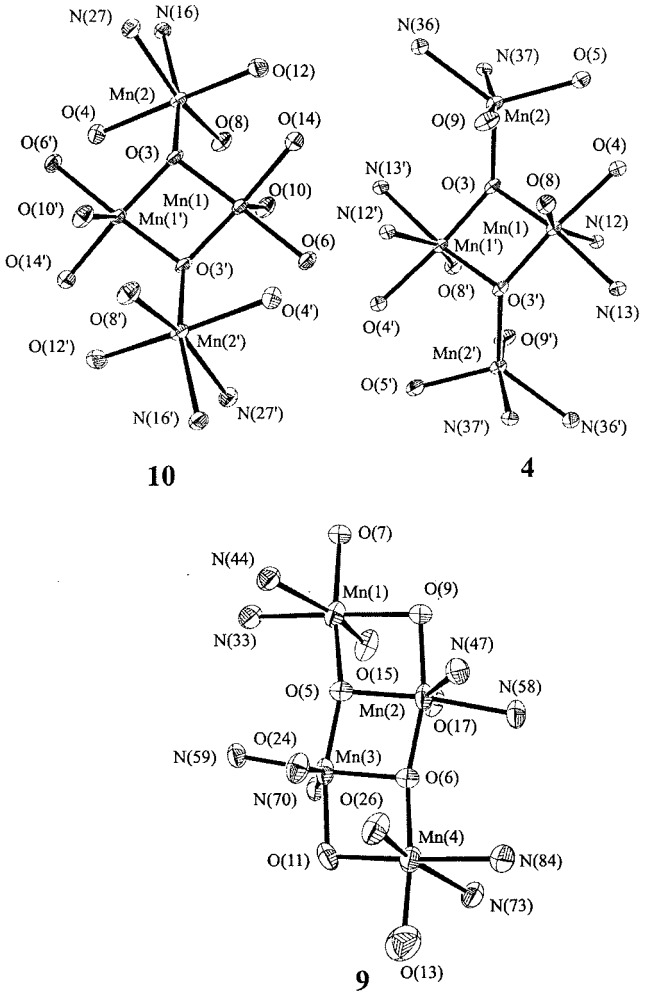

Figure 3. Cores of $[Mn_4O_2(O_2CMe)_6(bpy)_2]$ (**10**), the $[Mn_4O_2(O_2CMe)_4L_2]^{2+}$ cation of **4**, and the $[Mn_4O_2(OMe)_3(O_2CPh)_2L_2(MeOH)]^{2+}$ cation of **9**.

Table 4. Structural Comparison[a] of the $[Mn_4(\mu_3\text{-}O)_2]$ Cores of Complexes **4**, **9**, and **10**

parameter	**10**	**4**	**9**[b]
$Mn^{II}\cdots Mn^{III}$	3.287	3.208	2.991[c]
	3.481	3.362	
$Mn^{III}\cdots Mn^{III}$	2.778	2.784	2.810
$Mn^{II}-O-Mn^{III}$	112.36	111.92	99.92
	122.99	136.60	156.46
$\Delta(Mn^{II}-O-Mn^{III})$	10.63	24.68	56.54
$Mn^{III}-O-Mn^{III}$	97.12	97.00	96.37
$O-Mn^{III}-O$	88.88	83.00	83.57

[a] In units of Ångstroms and degrees. [b] Values averaged under virtual C_i symmetry. [c] Mn(1)···Mn(2).

that of previously reported $[Mn_4O_2(O_2CMe)_6(bpy)_2]$ (**10**).[19] The latter has a more symmetric, butterfly-like core compared with either **4** or **9**, but otherwise, there are strong similarities; these can be seen in Figure 3 and Table 4 where the cores of the three complexes are compared. In **4** and **10**, both long and short Mn···Mn separations are present, corresponding to mono- and dioxide-bridged separations, respectively. In contrast, the extra monoatomic bridges provided by the

(19) Vincent, J. B.; Christmas, C.; Chang, H. R.; Li, Q.; Boyd, P. D. W.; Huffman, J. C.; Hendrickson, D. N.; Christou, G. *J. Am. Chem. Soc.* **1989**, *111*, 2086.

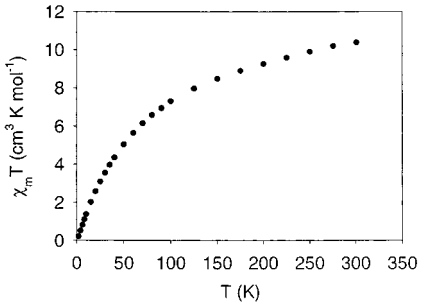

Figure 4. Plot of $\chi_M T$ vs temperature for complex **5**. χ_M is the dc magnetic susceptibility measured in a 10 kG field.

MeO^- groups in **9** make the Mn···Mn separations all much more similar, as well as distort the structure to a four-rung ladder motif. The latter also has a major effect on the two Mn−O−Mn[20] angles at each triply bridging oxide ion: the difference Δ is only 10.63° in **10**, but it increases in **4** and **9** to 24.68° and 56.54°, respectively. As a result, the geometry at the μ_3-O^{2-} ions is distinctly T-shaped in **9** rather than Y-shaped as in **4** and **10**.

It is also relevant to the magnetochemical discussion (see later) to note that **4** and **10** differ in an important way with respect to the arrangement of the bridging groups between each Mn(II)Mn(III) pair. In **10**, the two Mn(II)Mn(III) pairs at each triply bridging oxide are bridged similarly, one of them, for example, Mn(1)Mn(2), being bridged by two carboxylate groups, and the other, Mn(1′)Mn(2), being bridged by one. In complex **4**, however, the bridging ligands (two carboxylates and the ligand L) are all on the same side of the oxide (e.g., bridging Mn(1)Mn(2)), making the two sides very different. Thus, we prefer to describe **4** and **10** as possessing dimer-of-dimers and butterfly-like cores, respectively.

Direct Current Magnetic Susceptibility Studies. Direct current magnetic susceptibility data were collected in the 2.00−300 K range on powdered microcrystalline samples of **5**·2MeCN and **9**·2H_2O restrained in eicosane to prevent torquing.

The $\chi_M T$ versus T data for complex **5** are shown in Figure 4. For complex **5**, $\chi_M T$ per molecule smoothly decreases from 10.38 cm^3 K mol^{-1} at 300 K to 0.20 cm^3 K mol^{-1} at 2 K. The value at 300 K is less than the 14.75 cm^3 K mol^{-1} spin-only value ($g = 2.0$) expected for a 2Mn(II), 2Mn(III) complex with noninteracting metal centers, indicating the presence of appreciable antiferromagnetic interactions between the manganese ions. The $[Mn_4O_2]^{6+}$ core of **5** is expected to be similar to that of **4**, which has idealized C_i symmetry. This requires three exchange parameters to describe the pairwise exchange interactions between the metal centers, $J_{12} = J_{1'2'}$, $J_{1'2} = J_{12'}$, and $J_{11'}$, where J_{ij} refers to the Mn labeling of Figure 1; a fourth exchange parameter $J_{22'}$, describing the interaction between the two Mn(II) atoms, is taken as zero given the long distance between these metal ions. The Heisenberg spin Hamiltonian that describes the possible pairwise interactions is given by eq 4, where S_i represents the spin of metal Mn(i).

$$H = -2J_{11'}\hat{S}_1\hat{S}_{1'} - 2J_{12}(\hat{S}_1\hat{S}_2 + \hat{S}_{1'}\hat{S}_{2'}) - 2J_{12'}(\hat{S}_1\hat{S}_{2'} + \hat{S}_{1'}\hat{S}_2) \quad (4)$$

The overall degeneracy of this system is 900, made up of 110 individual spin states with total spin (S_T) values $S_T = 0-9$. A full matrix diagonalization approach for obtaining the eigenvalues of this spin Hamiltonian would require diagonalization of a 900 × 900 matrix. Unfortunately, the more convenient Kambe vector coupling method[21] is not applicable to this C_i symmetry molecule. In a previous report for complex **10**,[19,22,23] we applied a simplifying approximation by considering the $[Mn_4O_2]$ core to have effective C_{2v} symmetry, corresponding to $J_{12} = J_{12'} = J_{1'2} = J_{1'2'} = J'$, which makes the Kambe method applicable; this was reasonable because, as stated earlier, the $[Mn_4O_2]$ core of **10** is more symmetric that that of **5**, and all Mn(II)Mn(III) pairs are bridged by at least one carboxylate bridge, with the result that all Mn(II)Mn(III) interactions are expected to be similar. This simplifying approximation was also used to analyze the exchange interactions within the $[Mn_4O_2]^{6+,8+}$ cores of other tetranuclear complexes, which have idealized C_{2v} core symmetry.[2f,14,23b,24] For complex **5**, however, it was not considered reasonable to assume a C_{2v} model with $J_{12} = J_{12'} = J_{1'2} = J_{1'2'}$, given (i) the greater asymmetry of **5** versus **10**; (ii) the fact that the Mn(1)Mn(2) are bridged by an oxide, two carboxylates, and the L ligand, whereas Mn(1′)Mn(2) are bridged only by the oxide; and (iii) the Mn^{III}−O (oxide) bonds between the two halves of the molecule (Mn(1′)−O(3) = Mn(1)−O(3′) = 1.879(1) Å) are significantly lengthened compared with the others (Mn(1)−O(3) = Mn(1′)−O(3′) = 1.839(1) Å). Thus, efforts were restricted only to identifying the ground state of complex **5**.

The low-temperature behavior in Figure 4 suggests an $S = 0$ (or 1) ground state for **5**. Because the complex contains Mn(II) and the exchange interactions are consequently expected to be very weak, clear identification of the ground state by magnetization versus field data would be precluded by the low-lying excited states of greater S value crossing with the ground state in the applied fields of several Tesla. Thus, the ac susceptibility technique was employed.[7,25] In this technique, the sample is exposed to a very weak field (typically 1−5 G) oscillating at frequencies up to 1500 Hz.

(20) In complexes **5** and **10**, there are two Mn(II)Mn(III) pairs. In complex **9**, one oxide is bridging Mn(II), 2Mn(III), while the other is bridging 3Mn(III).

(21) Kambe, K. *J. Phys. Soc. Jpn.* **1950**, *5*, 48.
(22) Albela, B.; Sallah el Fallah, M.; Ribas, J.; Folting, K.; Hendrickson, D. N.; Christou, G. *Inorg. Chem.* **2001**, *40*, 1037.
(23) (a) Wemple, M. W.; Tsai, H. L.; Claude, J. P.; Wang, S.; Streib, W. E.; Hendrickson, D. N.; Christou, G. *J. Chem. Soc. Chem. Commun.* **1996**, *35*, 6437. (b) Vincent, J. B.; Christmas, C.; Chang, H. R.; Li, Q.; Boyd, P. D. W.; Huffman, J. C.; Hendrickson, D. N.; Christou, G. *J. Am. Chem. Soc.* **1989**, *111*, 2026.
(24) (a) Tsai, H. L.; Wang, S.; McCusker, J. K.; Schmitt, W. E.; Hendrickson, D. N.; Christou, G. *Inorg. Chem.* **1991**, *30*, 305. (b) Sessoli, R.; Tsai, H. L.; Schake, A. R.; Wang, S.; Vincent, J. B.; Folting, K.; Hendrickson, D. N.; Gatteschi, D.; Christou, G. *J. Am. Chem. Soc.* **1993**, *115*, 1804. (c) McCusker, J. K.; Tang, H. G.; Wang, S.; Christou, G.; Hendrickson, D. N. *Inorg. Chem.* **1992**, *31*, 1874.
(25) Novak, M. A.; Sessoli, R. In *Quantum Tunneling of Magnetization-QTM'94*; Gunther, L., Barbara, B., Eds.; Kluwer: Amsterdam, 1995; pp 171−188.

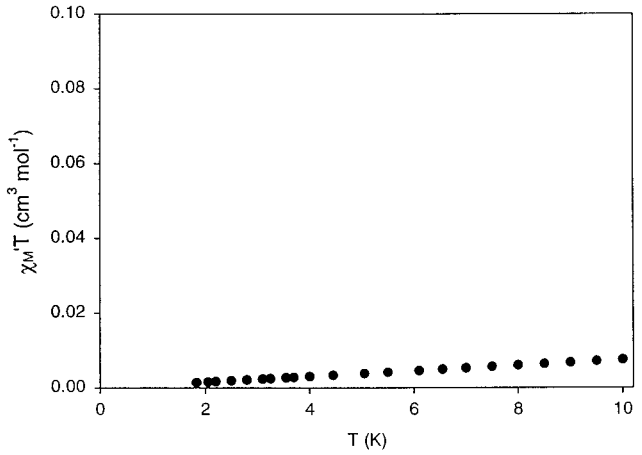

Figure 5. Plot of $\chi_M'T$ vs temperature for complex **5** in the 2−10 K temperature range. χ_M' is the ac magnetic susceptibility measured in a 3.5 G oscillating field.

In cases when the magnetization of the sample can relax (reorient) rapidly enough to keep in phase with the oscillating field, then the magnitude of the "in-phase" ac susceptibility (χ_M') is equal to the dc susceptibility (χ_M). This is a good way to prevent problems associated with application of large dc fields. In Figure 5 is shown the χ_M' of **5**, plotted as $\chi_M'T$ versus T, at low temperature to minimize the possibility of populating excited states. The very low values of $\chi_M'T$ indicate an $S = 0$ ground state for **5**; an $S = 1$ ground state is expected to give a $\chi_M'T$ value of 1.00 cm^3 mol^{-1} K for $g = 2$.

An $S = 0$ ground state is that expected for **5** with antiferromagnetic exchange interactions and $|J_{11'}| > |J_{12}| = |J_{1'2'}| > |J_{12'}| = |J_{1'2}|$, giving the spin alignments as shown. This is consistent with the structural asymmetry mentioned previously, that is, that *all* bridging ligands bridge across the Mn(1)Mn(2) and Mn(1′)Mn(2′) pairs, and the presence of a small but significant difference in the Mn−O(oxide) bond distances, both leading to a significant difference in the corresponding Mn(II)Mn(III) exchange interactions, that is, $|J_{12}| = |J_{1'2'}| > |J_{12'}| = |J_{1'2}|$.

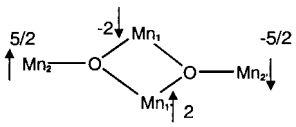

The χ_MT versus T data for complex **9** are shown in Figure 6. The χ_MT value per molecule gradually decreases from 8.32 cm^3 K mol^{-1} at 300 K to 6.79 cm^3 K mol^{-1} at 50 K and then sharply decreases to 5.21 cm^3 K mol^{-1} at 5.0 K. The χ_MT value at 300 K is less than 13.38 cm^3 K mol^{-1}, the spin-only ($g = 2$) value expected for a Mn(II), 3Mn(III) cluster with noninteracting metal ions. This suggests the presence of antiferromagnetic interactions in **9**. The χ_MT value at 50 K suggests an $S = {}^7/_2$ ground state, with the sharp decrease observed at lower temperatures most likely because of zero-field splitting effects and perhaps weak intermolecular interactions mediated by the π-stacking of the bipyridine rings observed in the crystal structure.

The spin Hamiltonian for the cation of **9** with C_1 symmetry is given in eq 5, using the atom labeling of Figure 2. The

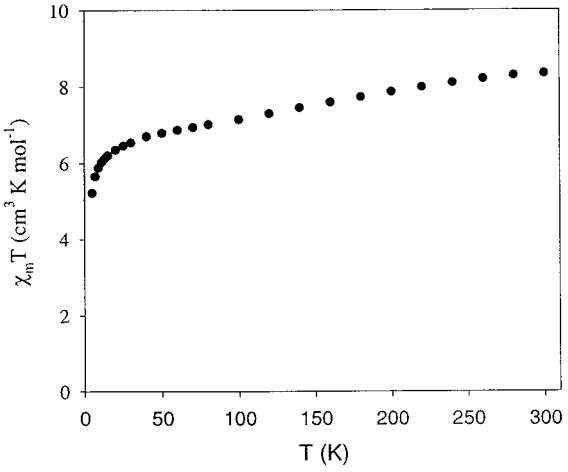

Figure 6. Plot of χ_MT vs temperature for complex **9**. χ_M is the dc magnetic susceptibility measured in a 10 kG field.

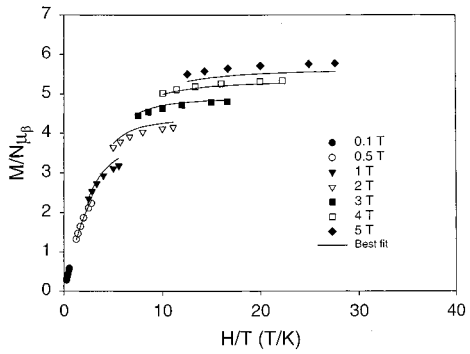

Figure 7. Plot of $M/N\mu_B$ vs H/T for complex **9** in eicosane at 1, 5, 10, 20, 30, 40, and 50 kG. The solid lines are fits using the appropriate method; see the text for the fitting parameters.

degeneracy of this system is 750, made up of 109 individual spin states ranging from $S_T = {}^1/_2$ to ${}^{17}/_2$.

$$H = -2J_{23}\hat{S}_2\hat{S}_3 - 2J_{12}\hat{S}_1\hat{S}_2 - 2J_{24}\hat{S}_2\hat{S}_4 - 2J_{13}\hat{S}_1\hat{S}_3 - 2J_{34}\hat{S}_3\hat{S}_4 \quad (5)$$

As for **5**, a simplifying approximation was not considered reasonable given the large difference in angles at the bridging oxide ions, and no attempt was made to determine the values of the five inequivalent J values in this complex. Instead, dc magnetization data at low temperatures were used to identify the spin ground state of **9**. The expected stronger exchange coupling between the metal ions in **9** due to each Mn_2 pair being bridged by two monatomic bridges instead of only one as in **4**/**5** suggested that low-lying excited states would not be a problem in this case.

Direct current magnetization data were collected in the 2.0−30 K and 1−5 T ranges and are shown in Figure 7 as $M/N\mu_B$ versus H/T plots, where N is Avogadro's constant and μ_B is the Bohr magneton. The nonsuperposition of the various isofield lines clearly indicates significant zero-field splitting (ZFS) in **9**. The data were fit using the matrix diagonalization method described elsewhere,[26] which assumes that only the ground state is populated. The best fit was obtained with the following parameters: $S = {}^7/_2$, $D =$

(26) *MAGNET*; Davidson, E. R.; Indiana University: Bloomington, IN.

-0.77 cm^{-1}, and $g = 1.79$, where D is the axial ZFS parameter. The fit is shown as the solid lines in Figure 7. Attempts to fit the data with $S = {}^5/_2$ or ${}^9/_2$ gave unreasonable values of g of 2.5 and 1.4, respectively, and these possibilities were therefore discounted. The $S = {}^7/_2$ ground-state value is also supported by the ac data (vide infra).

Alternating Current Magnetic Susceptibility Studies. The large spin value and appreciable ZFS in the ground state for **9** raised the possibility that **9** would behave as an SMM. Alternating current susceptibility experiments were therefore performed to determine whether **9** would exhibit slow magnetization relaxation. The ac susceptibility technique applies a weak (usually 1−5 G), oscillating magnetic field to a sample, using oscillation frequencies typically up to 1500 Hz.[7,25] This provides a convenient method to investigate the magnetization relaxation rate of a complex. As described previously, for species with fast relaxation rates, the magnetization will be in phase with the oscillating field, and the measured in-phase signal (χ_M') will be equal to the dc susceptibility (χ_M). For such species, the out-of-phase signal (χ_M'') is therefore zero. For species with slow relaxation rates, the magnetization cannot keep in phase with the oscillating field, χ_M' decreases, and a corresponding nonzero value of χ_M'' is obtained. The precise temperature at which the latter is a maximum depends on the field oscillation frequency. Such frequency-dependent χ_M'' signals are the diagnostic signature of superparamagnetic mesoscale magnetic particles and also of single-molecule magnets (SMMs), both of which have slow magnetization relaxation rates (compared with paramagnets). In addition, at the temperature of the χ_M'' peak maximum, the magnetization relaxation rate is equal to the oscillation frequency of the applied field. This provides kinetic data that can be employed to obtain the activation energy barrier to magnetization relaxation (reversal).

Powdered polycrystalline samples of **5** and **9** were studied in the 1.7−12 K temperature range with a 3.5 G ac field oscillating at 500, 1000, and 1500 Hz. As implied previously, complex **5** does not show an out-of-phase (χ_M'') ac susceptibility signal, as expected for a compound with a spin ground state of $S = 0$. For complex **9**, however, there is evidence at temperatures below 3 K of slow magnetization relaxation. In Figure 8 are shown the χ_M' (top, plotted as $\chi_M'T$) and χ_M'' (bottom) signals. The value of $\chi_M'T$ decreases from 6.45 cm^3 K mol^{-1} at 3.0 K to 6.00 cm^3 K mol^{-1} at 1.7 K, and this is accompanied by the appearance of a frequency dependent χ_M'' signal. The peak maxima clearly lie at temperatures lower than the 1.7 K minimum accessible by the instrument. The plateau value of $\chi_M'T$ of ∼6.6 cm^3 K mol^{-1} at $T > 4$ K, where the relaxation is in phase with the oscillating field and $\chi_M'T$ (ac) $= \chi_MT$ (dc), corresponds to that expected for $S = {}^7/_2$ and $g = 1.83$, in good agreement with the dc magnetization fit ($S = {}^7/_2$, $g = 1.79$).

The ac susceptibility data indicate that complex **9** displays slow magnetization relaxation characteristic of an SMM, and this is consistent with its relatively large ground-state spin value of $S = {}^7/_2$ and significant zero-field splitting as reflected in the $D = -0.77$ cm^{-1} $= -1.11$ K value obtained from the dc magnetization fits described previously. The potential

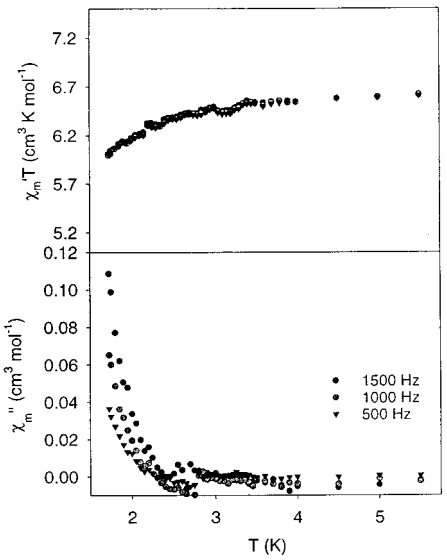

Figure 8. Plots of (top) the in-phase χ_M' signal as $\chi_M'T$ and (bottom) out-of-phase χ_M'' signal vs temperature for complex **9** in eicosane in a 3.5 G ac field oscillating at 1500, 1000, and 500 Hz.

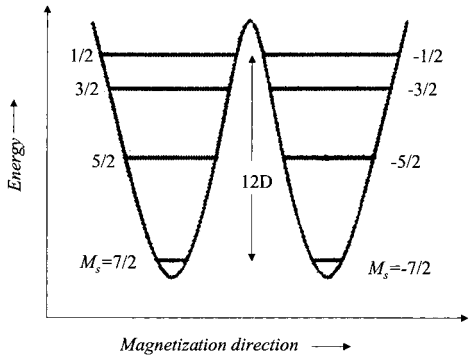

Figure 9. Plot of potential energy vs the magnetization direction for a molecule with an $S = {}^7/_2$ spin ground state in zero magnetic field. Axial zero-field interactions split the $S = {}^7/_2$ state into $M_s = \pm{}^7/_2, \pm{}^5/_2, \pm{}^3/_2, \pm{}^1/_2$ levels.

energy barrier to magnetization relaxation is the energy difference between the $M_s = \pm{}^7/_2$ and $M_s = \pm{}^1/_2$ levels, which is $(S^2 - {}^1/_4)|D|$, or 9.24 cm^{-1} (13.3 K). This is summarized in Figure 9, which shows a plot of the potential energy of a molecule with $S = {}^7/_2$ exhibiting easy-axis-type anisotropy (negative D value) as its magnetization vector changes from spin "up" ($M_s = -{}^7/_2$) to spin "down" ($M_s = +{}^7/_2$) via intermediate orientations. The ac susceptibility data of Figure 8 identify complex **9**·2H$_2$O as a new member of the SMM family. Further studies at temperatures below 1.7 K will now be necessary in order to determine the precise magnetization relaxation rate and to observe hysteresis loops and associated behavior.

Conclusions

The reactions of manganese carboxylate complexes with ligand L have been explored and found to give two families of complexes with formulas $[Mn_4O_2(O_2CR)_4L_2](ClO_4)_2$ and $[Mn_4O_2(OMe)_3(O_2CR)_2L_2(MeOH)](ClO_4)_2$ (R = Me, Et, Ph) depending on the solvent. The two types can be interconverted under the appropriate conditions. The methoxide-

bridged species has an interesting four-rung ladder core not seen before in Mn chemistry, similar to that in a related Fe(III) complex with L.[10] Its magnetic properties are also interesting; the complex has a relatively large ground-state spin value of $S = {}^{7}/_{2}$ that, together with a significant magnetoanisotropy as gauged by the D value of -0.77 cm^{-1}, leads to slow magnetization relaxation rates and resulting single-molecule magnetism behavior. Further studies at lower temperatures are planned to investigate magnetization hysteresis loops and the possible presence of quantum tunneling of the magnetization, which will be manifested as steps on the loops.[27]

(27) (a) Sangregorio, C.; Ohm, T.; Paulsen, C.; Sessoli, R.; Gatteschi, D. *Phys. Rev. Lett.* **1997**, *78*, 4645. (b) Aubin, S. M. J.; Dilley, N. R.; Pardi, J.; Krzystek, J.; Wemple, M. W.; Brunel, L. C.; Maple, M. B.; Christou, G.; Hendrickson, D. N. *J. Am. Chem. Soc.* **1998**, *120*, 4991. (c) Hendrickson, D. N.; Christou, G.; Ishimoto, H.; Yoo, J.; Brechin, E. K.; Yamaguchi, A.; Rumberger, E. M.; Aubin, S. J.; Sun, Z.; Aromi, G. *Polyhedron* **2001**, *20*, 1479.

The results of this work demonstrate that the bis-bipyridyl ligand L can provide access to new Mn clusters with interesting properties not seen previously with smaller chelating ligands such as bpy; this is analogous to previous results obtained from the use of L in Fe and Co chemistry. Clearly, the use of other poly-pyridyl or related ligands offers a potential route to other new polynuclear metal clusters, and such studies are continuing.

Acknowledgment. This work was supported by NIH and NSF grants to G.C. and D.N.H.

Supporting Information Available: X-ray crystallographic files in CIF format for complexes **4**·2THF and **9**·3MeOH·H_2O. This material is available free of charge via the Internet at http://pubs.acs.org.

IC011262K